A major purpose of the Technical Information Center is to provide the broadest dissemination possible of information contained in DOE's Research and Development Reports to business, industry, the academic community, and federal, state and local governments.

Although a small portion of this report is not reproducible, it is being made available to expedite the availability of information on the research discussed herein.

LA-UR-88-3793

Los Alamos National Laboratory is operated by the University of California for the United States Department of Energy under contract W-7405-ENG-36.

LA-UR--88-3793

DE89 003484

TITLE: **OPTICAL TRANSITION RADIATION MEASUREMENTS FOR THE LOS ALAMOS AND BOEING FREE-ELECTRON LASER EXPERIMENTS**

AUTHOR(S): **A. H. Lumpkin, P-15**
R. B. Feldman, AT-6
D. W. Feldman, and S. A. Apgar, and B. E. Carlsten, AT-7
R. B. Fiorito and D. W. Rule, NSWC, Silver Spring, Maryland

SUBMITTED TO: **The Tenth International Free Electron Laser Conference, August 29 - September 2, 1988, Jerusalem, Israel**

Los Alamos

Los Alamos National Laboratory
Los Alamos, New Mexico 87545

DISCLAIMER

OPTICAL TRANSITION RADIATION MEASUREMENTS FOR THE LOS ALAMOS AND BOEING FREE-ELECTRON LASER EXPERIMENTS

A.H. Lumpkin, R. B. Feldman, D. W. Feldman, S. A. Apgar, and B. E. Carlsten
Los Alamos National Laboratory
Los Alamos, New Mexico 87545, U.S.A.
and
R. B. Fiorito and D. W. Rule
Naval Surface Warfare Center
Silver Spring, Maryland 20903-5000, U.S.A.

Abstract

Optical transition radiation (OTR) measurements of the electron-beam emittance have been performed at a location just before the wiggler in the Los Alamos Free-Electron Laser (FEL) experiment. Beam profiles and beam divergence patterns from a single macropulse were recorded simultaneously using two intensified charge-injection device (CID) television cameras and an optical beamsplitter. Both single-foil OTR and two-foil OTR interference experiments were performed. Preliminary results are compared to a reference variable quadrupole, single screen technique. New aspects of using OTR properties for pointing the e-beam on the FEL oscillator axis, as well as measuring e-beam emittance are addressed.

I. INTRODUCTION

Characterization of the electron beam driving a Free-Electron Laser (FEL) is an important aspect of optimizing such systems. In particular, good electron-beam emittance can be a critical issue ensuring spatial overlap of the optical and electron beams in the wiggler. An effective, newly developed technique for measuring electron-beam emittance on a single macropulse (and perhaps a few micropulses) of the high-current, high-energy electron beams uses the unique properties of optical transition radiation (OTR). This radiation is emitted when a charged-particle beam transits an interface between two media of different dielectric constants. Radiation is emitted in both forward and backward directions. The backward lobe is a function of the Fresnel reflection coefficients so that detection at 90° to the beam direction is practical [1-3]. Preliminary beam-profile measurements at the Los Alamos FEL were reported previously [4], and the applicability to the FELs is also addressed in Reference 5.

Two sets of measurements were successfully performed at Los Alamos. Beam profiles and beam-divergence patterns from a single screen were recorded using two intensified charge-injection device (CID) television cameras and an optical beamsplitter. Data were recorded with and without polarization effects on both x and y axes. The separation and width of the OTR angular distribution lobes ($\theta \sim 1/\gamma$) agreed with the measured electron-beam energy. Preliminary analysis of the data yielded results consistent with the expected divergence of a few mrad. The beam-spot detector was also used in conjunction with the standard technique of varying the fields in a quadrupole doublet and measuring the spatial profiles. These data will allow a comparison of the OTR single-shot technique to the multishot quad-scan results. A two-foil OTR interference experiment was also performed. The comparison of these various emittance measurements will be discussed. Based on these results and further calculations, an OTR experiment for the Boeing FEL is being planned.

II. TRANSITION RADIATION EXPERIMENTAL PROCEDURES

As mentioned briefly in the introduction, OTR's unique properties can be exploited to provide minimally intercepting (thin foil or film) electron-beam diagnostics for position and profile, intensity, emittance, and energy on a single macropulse. Figure 1 shows the qualitative OTR patterns for normal and oblique incidence as compared to Cherenkov radiation. When the OTR foil is at 45° to the beam; the radiation is emitted in an annular pattern around a ray at 90° to the beam direction, a standard viewing port geometry. In Fig. 2 the angular distribution pattern is displayed in more detail, and the lobe features include an opening angle θ_p proportional to $1/\gamma$, a peak intensity proportional to γ^2, a lobe-width proportional to e-beam divergence (emittance), and a spectral function proportional to $1/\lambda^2$ for an aluminium foil for example.

The experiment was fielded at a position just before the wiggler in the Los Alamos FEL experiment as shown in Fig. 3. A 60° achromatic bend brings the 20 MeV e-beam onto the oscillator axis. Viewing ports on either side of the quadrupole doublet (Q3) before the wiggler and screens at either end of the wiggler were used to align the beam with the laser reference on the oscillator axis. It is noted that for FELs an alignment laser often exists for this purpose. In this case, the same alignment laser is specularly reflected from the OTR foil and used to align the two intensified CID television cameras. A large diameter pellicle splits the OTR. Retroflections of the alignment laser off the camera sensors, intensifier entrance window, and the front surface of the two Nikon 85 mm, f/1.4 lenses were used to align the detectors to about 1 mrad accuracy. A special object at infinity source was used to focus the angular distribution camera [2], while fiducials at the OTR foil object plane were used to focus the

other camera. The sensors were adjusted so that the laser spot was detected in the central channel (x and y) position of the data-acquisition system. A remotely operated shutter and linear polarizer were placed at the exit port for the OTR source.

Figure 4 schematically shows how both the spatial intensity (beam spot profile) and the OTR angular distribution pattern can be recorded by focussing at the image plane and the focal plane (infinity), respectively. The spatial calibration was based on known fiducials in the object plane while the angular sensitivity was determined by deflecting a small laser beam with a motor-driven mirror and recording the mirror angle change and the pixel position of the spot in the microcomputers.

We nominally operated with about a 30-μs-long macropulse, 46-ns micropulse spacing, and ~1.2 nC/micropulse, and minimal magnetic bunching in the 60° bend. This implies the micropulse duration was about 25 ps and our peak currents were about 50A and average currents were about 0.7μA. Towards the end of the runs, we lengthened the macropulse to 100μs, increased the charge to 3 nC/micropulse, and bunched to our limit of about 10 ps. In this mode, the peak-current was ~300A and the average was 6μA. The OTR foils were polished molybdenum, aluminized fused silica, and 7.6 μm-thick Kapton.

III. EXPERIMENTAL RESULTS AND PRELIMINARY CALCULATIONS

Data were obtained with both single-foil and two-foil setups and with several different e-beam focusing conditions and average currents. Due to space limitations only a few examples will be shown. It is highly probable that our simple assumptions on the electron-beam distributions will have to be modified to account for a core of good quality beam (lower emittance) superimposed with a halo of poor-quality beam (high emittance). Also, the present calculation does not include energy spread effects.

Figure 5 is a composite figure showing single-foil OTR data for both beam divergence and beam profiles. The beam was focussed to an x-waist and the linear polarizer was oriented horizontally. The images are shown in the upper two quadrants and the profiles are displayed in the two lower quadrants. In the lower left quadrant, the characteristic lobe-structure of $I_{\parallel}$ is seen on the horizontal axis and $I_{\perp}$ for a vertical scan is shown on the vertical axis. The x and y-beamspot profiles are seen in the lower right quadrant. Figure 6 shows a comparison of the data in Fig. 5 to a calculation for E = 20 MeV and the rms x-component of beam divergence of 4.9 mrad obtained from a least-squares fitting routine. The two lobe peaks can be seen at approximately ±25 mrad as expected for $\gamma = 41$. There are some deviations between the two curves, and as mentioned in the opening of this section, this is a preliminary analysis.

The x-component of emittance, ϵ_x, calculated by using the above value of 4.9 mrad and the half width, half maximum intensity of the beamspot of 0.8 mm is $\epsilon_x = 4\pi$ mm mrad. Similar values were obtained for the y-component of emittance, ϵ_y.

For comparison to the OTR angular pattern result, we used the variation of the beam spot profile with quadrupole (Q3) field variation to determine emittance somewhat independently (but using OTR light for the profile determinations). Using the full-width-at-half-maximum (FWHM) spot-diameter values, we fit the data to the appropriate hyperbola. We obtained unnormalized emittances of $\epsilon_x = 1.5\pi$ mm mrad and $\epsilon_y = 1.1\pi$ mm mrad, where it is noted that in these cases the x and y waists were obtained separately. We did not observe such small values when we tried to focus simultaneously in x and y, nor when we ran at the higher peak current mode described in section II. The underlying assumption of the quadrupole focusing method is a uniform density ellipse in phase space, while the analysis of the OTR angular distribution was based on a gaussian distribution of beam-particle angles at the beam waist. Reconciliation of these two distributions should account for most of the differences between the two measurements [6]. Finally, the actual beam distributions may need to be modeled more carefully for both emittance measurement techniques. Energy-spread effects should be included in that step.

A two-foil OTR interference experiment was also performed. The first foil was a thin, transparent (7.6 μm = 0.3 mil) Kapton film spaced 0.5 mm in front of the aluminized fused-silica screen. Figure 7 shows the predicted patterns for the parallel ($I_{||}$) and perpendicular ($I_{\perp}$) polarization components for this system at 45° to the beam and for divergences of 5.0 and 1.37 mrads. The latter value is an estimated lower limit for this assembly due to the beam scattering by the first foil. The predicted three fringes were observed with no filter, a 600-nm band pass filter, and with the polarizer oriented on both x and y axis. Figure 8 shows a horizontal profile through the experimental interference pattern with a 600 × 40 nm bandpass filter. Several files of data are still to be analyzed.

In regard to foil survivability issues, we have some preliminary results also. The aluminized fused-silica screen was bombarded for several hours a day for four days at the lower current mode (still about 600 micropulses per macropulse) with no observable damage. However, at the high mode (2000 micropulses, ~300A peak current), the aluminum flaked off in tens of minutes. This may have been partially a differential heating effect with the fused-silica substrate (which appeared undamaged). In the two-foil assembly, a similar experiment was performed. We observed no apparent damage to the Kapton front foil, and the aluminized fused silica was affected less than in its single foil tests over tens of minutes. Kapton foil

flatness or tautness may have altered during the low- to higher-current runs, but no significant effect on the interference pattern was observed.

As was noted in early OTR experiments by Wartski [7], the position of the central minimum of the OTR pattern is sensitive to the angle of interception of the electron beam with respect to the foil normal. Thus by adjusting the steering magnets and observing both the beam image and the angular distribution image with respect to the laser reference points, one can carefully align the e-beam with the alignment laser axis, which in our case was also the FEL oscillator axis. This technique was used in our experiments, and should considerably simplify FEL e-beam tuning for the wiggler region.

Finally, we briefly address our preliminary designs for the Boeing FEL experiment. Since the e-beam energy is 110 MeV, larger spacing between the interferometer foils is possible . Therefore, we will be able to look at the front face of the second foil directly. Predicted interferograms for several cases of beam divergence are shown in Fig. 9. The upper figure shows the 0.4 and 0.6 mrad for a foil spacing of 4 cm, and the lower figure shows the difference between 0.6 and 0.9 mrad for the foil spacing of 2 cm. In both cases, a bandpass filter at 450 nm was assumed. Our initial experiments may use thin carbon foils as the first foil and existing polished-aluminum mirrors as the second surface. Our e-beam "pointing" studies will also be done during these experiments.

IV. SUMMARY AND CONCLUSIONS

The OTR technique compares favorably with standard emittance diagnostics that rely on measurement sequences (quadrupole field variation) at one screen position or two screens. Several advantages for OTR are:

- Measurements are possible on a single macropulse (source strength permitting),
- Data structure and theory allow on-line evaluation of emittance,
- A single position in the beamline can be used for e-beam profile, divergence, and angle (pointing) measurements,
- Thinner screens (foils) reduce beam scattering and x-ray production, and
- OTR provides a simultaneous e-beam energy diagnostic (~1% accuracy).

Some disadvantages are related to source brightness, the required careful optical alignments, and convolution of divergence and energy effects. In the final analysis though,

OTR-based diagnostics should provide information vital to optimization of FEL performance and the validations of simulations of FEL experiments.

REFERENCES

1. L. Warski, et. al., J. Applied Phys. 46, 1975 3644.
2. R. B. Fiorito, et. al., Proc. 6th International Conference on High-Power Beams, Kobe, Japan, 1986.
3. D. W. Rule, "Transition Radiation Diagnostics for Intense Charged Particle Beams," Nucl. Inst. and Meth., B24/25, 1987 (901-904).
4. Alex H. Lumpkin, "Cherenkov and Transition Radiation Diagnostics for High-Energy Free-Electron Lasers," Presented at AIAA 19th Fluid Dynamics, Plasma Dynamics and Lasers Conference, June 8-10, 1987, Honolulu, Hawaii, AIAA 87-1358, LA-UR-87-1535.
5. X. K. Maruyama, R. B. Fiorito, and D. W. Rule, "Optical Transition Radiation as a Real-time, On-line Diagnostic for Free-Electron Laser Systems," Proceedings of the Ninth International FEL Conference, Williamsburg, Va., September 1987, Nucl. Instr. and Meth., A272, 237, October 1988.
6. Claude LeJeune and Jean Aubert, "Emittance and Brightness: Definitions and Measurements," Adv. in Electronics and Electron Physics, Suppl. 13A, 158-259, 1980.
7. L. Wartski, "Study on Optical Transition Radiation Produced by 30 to 70 MeV Energy Electrons. Application to the diagnosis of beams of charged particles," Ph.D. Thesis, Université de Paris - Sud, Centre d' Orsay, 1976 (unpublished).

Figure Captions

Fig. 1. A schematic representation of OTR and Cherenkov radiation patterns.

Fig. 2. A schematic representation of the OTR angular distribution pattern dependence on e-beam parameters where γ is the Lorentz factor..

Fig. 3. A schematic experimental setup for the OTR experiments on the Los Alamos FEL.

Fig. 4. A schematic representation of the focus at the object (beam spot) and focus at infinity (angular distribution) techniques.

Fig. 5. A composite of OTR single foil data showing both divergence and beam spot images (upper) and profiles (lower).

Fig. 6. A comparison of divergence data from Fig. 5 to a calculation with σ = 4.9 mrad.

Fig. 7. Predicted interferogram patterns for the Los Alamos case.

Fig. 8. Experimental profile for the interference experiment data exhibiting the expected three fringes.

Fig. 9. Predicted interferogram for several cases of e-beam divergence for the Boeing FEL case.

OPTICAL TRANSITION RADIATION PATTERNS

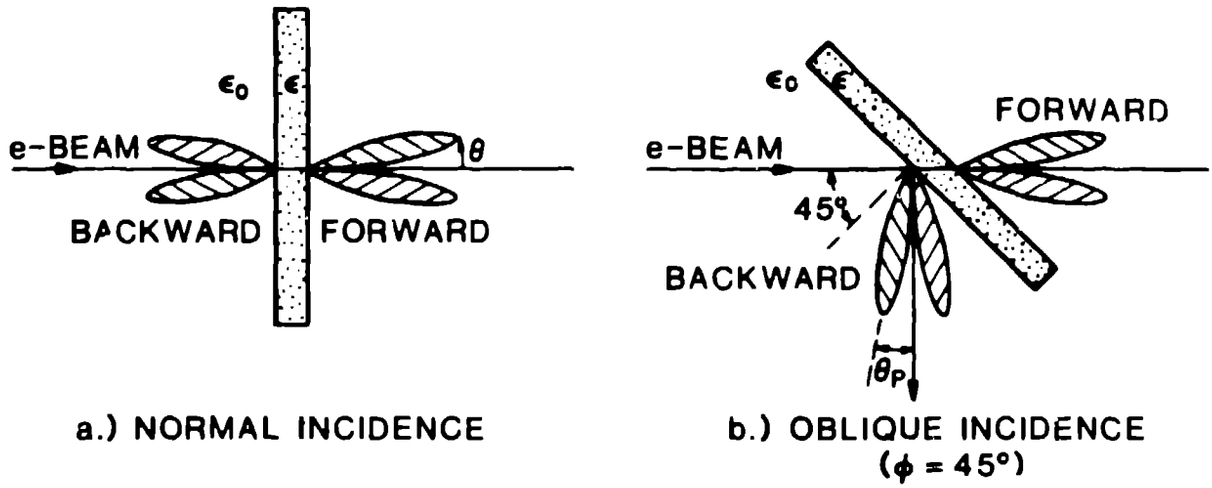

a.) NORMAL INCIDENCE

b.) OBLIQUE INCIDENCE ($\phi = 45°$)

CHERENKOV RADIATION PATTERN ($\theta \sim 46°$)

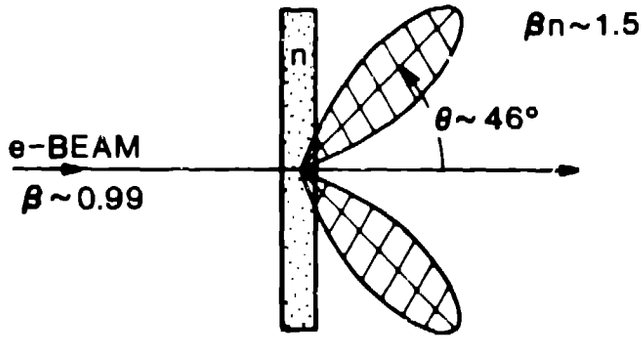

Fig. 1

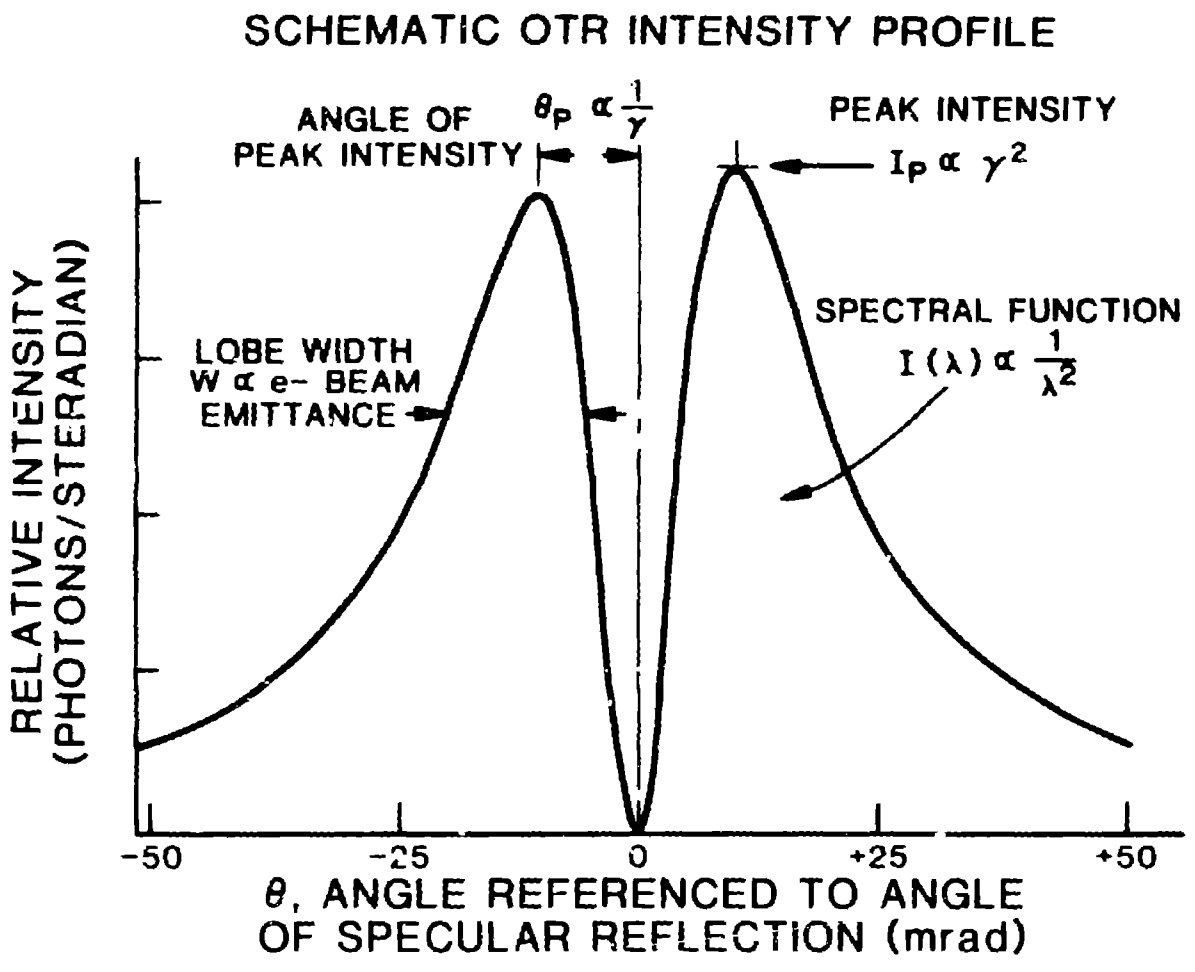
SCHEMATIC OTR INTENSITY PROFILE
ANGLE OF PEAK INTENSITY
$\theta_P \propto \frac{1}{\gamma}$
PEAK INTENSITY
$I_P \propto \gamma^2$
LOBE WIDTH
W ∝ e- BEAM EMITTANCE
SPECTRAL FUNCTION
$I(\lambda) \propto \frac{1}{\lambda^2}$
RELATIVE INTENSITY
(PHOTONS/STERADIAN)
-50
-25
0
+25
+50
θ, ANGLE REFERENCED TO ANGLE OF SPECULAR REFLECTION (mrad)

Fig. 2

Schematic of OTR Experiment
(Los Alamos)

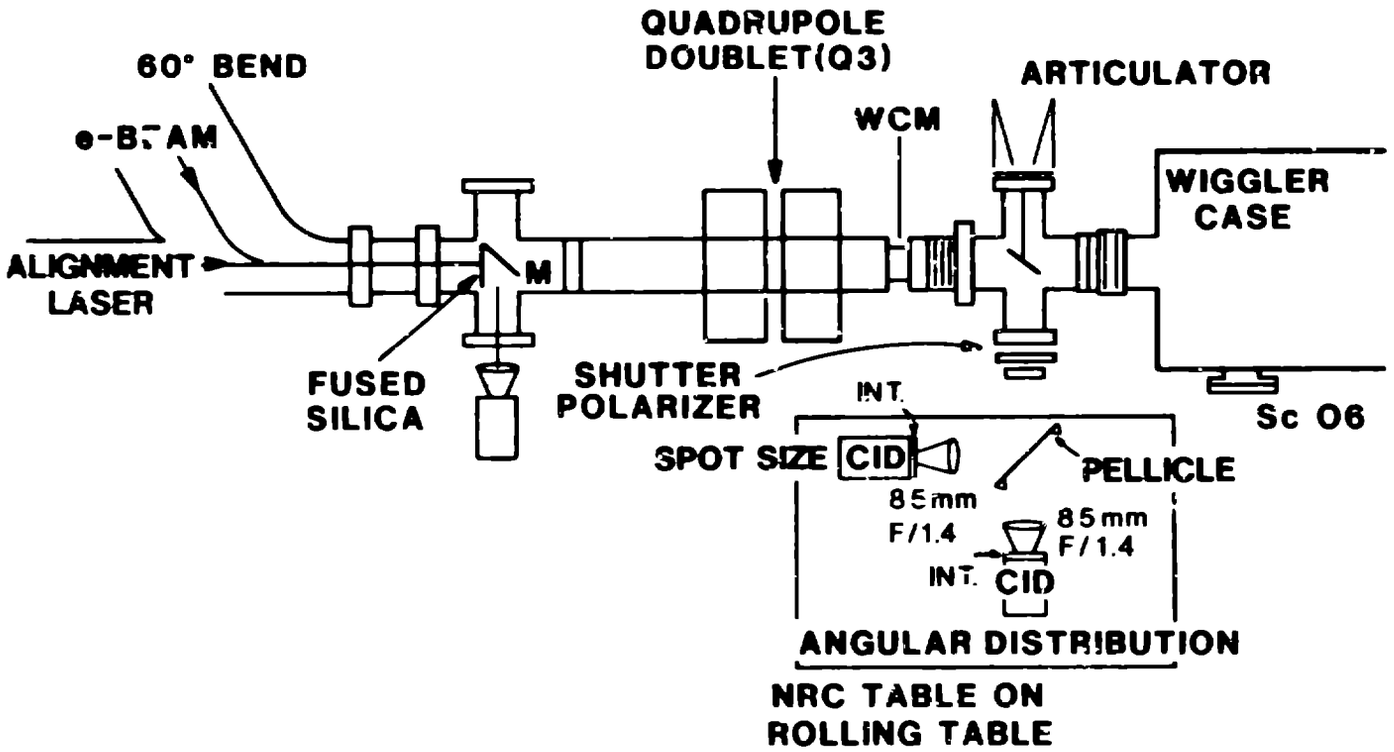

Fig. 3

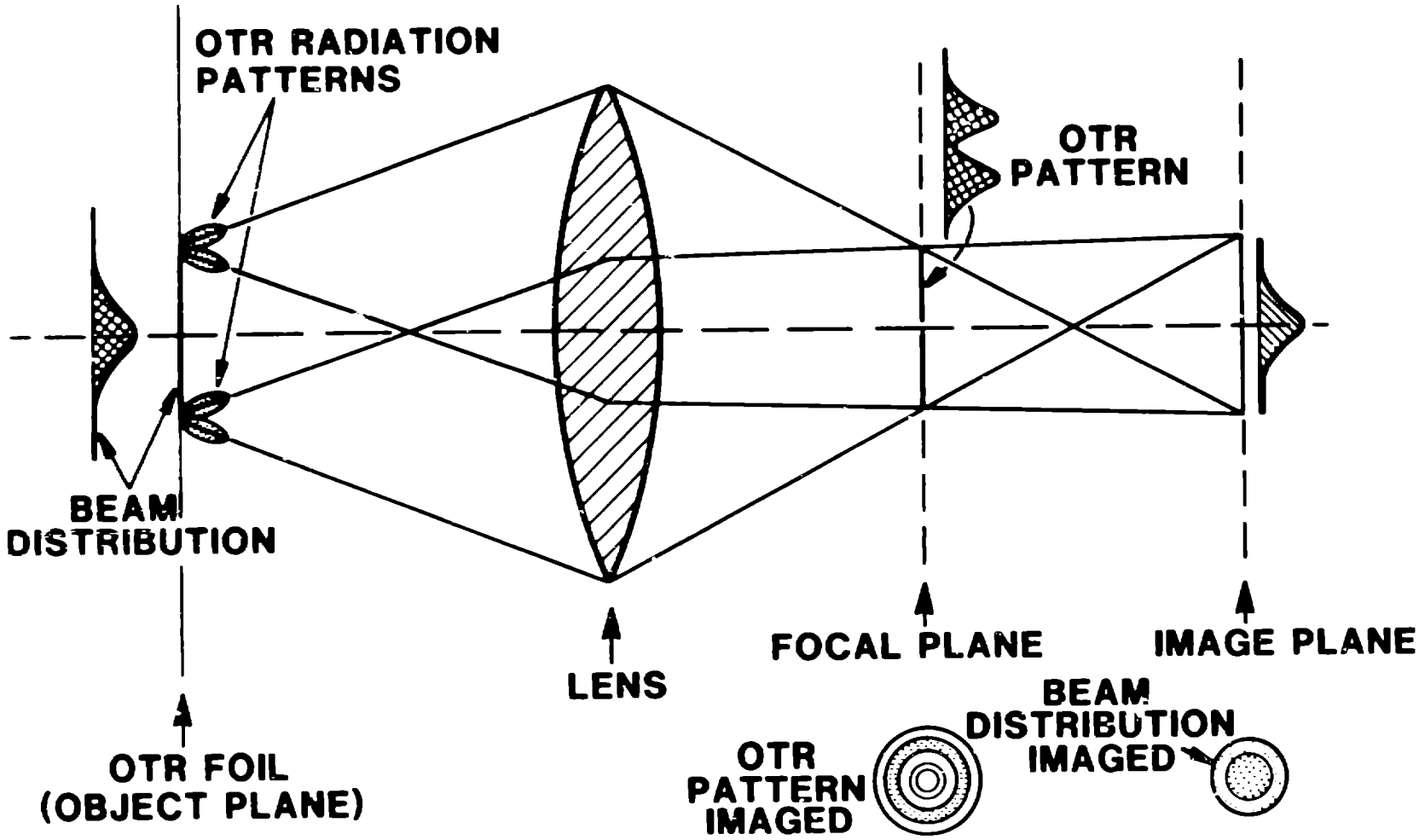
OTR RADIATION PATTERNS
OTR PATTERN
BEAM DISTRIBUTION
OTR FOIL (OBJECT PLANE)
LENS
FOCAL PLANE
IMAGE PLANE
BEAM DISTRIBUTION IMAGED
OTR PATTERN IMAGED

Fig. 4

Single Foil OTR Data

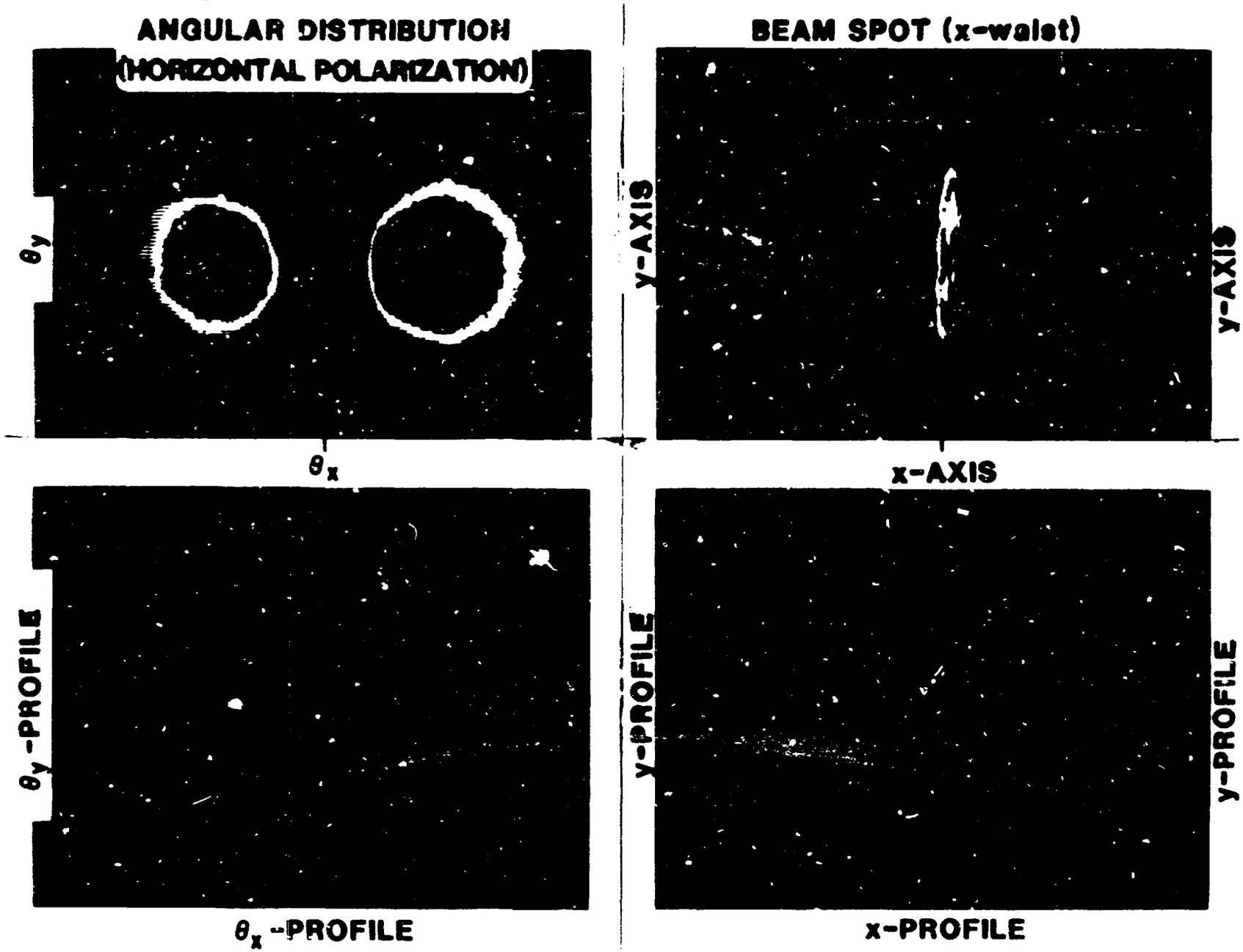

Fig. 5

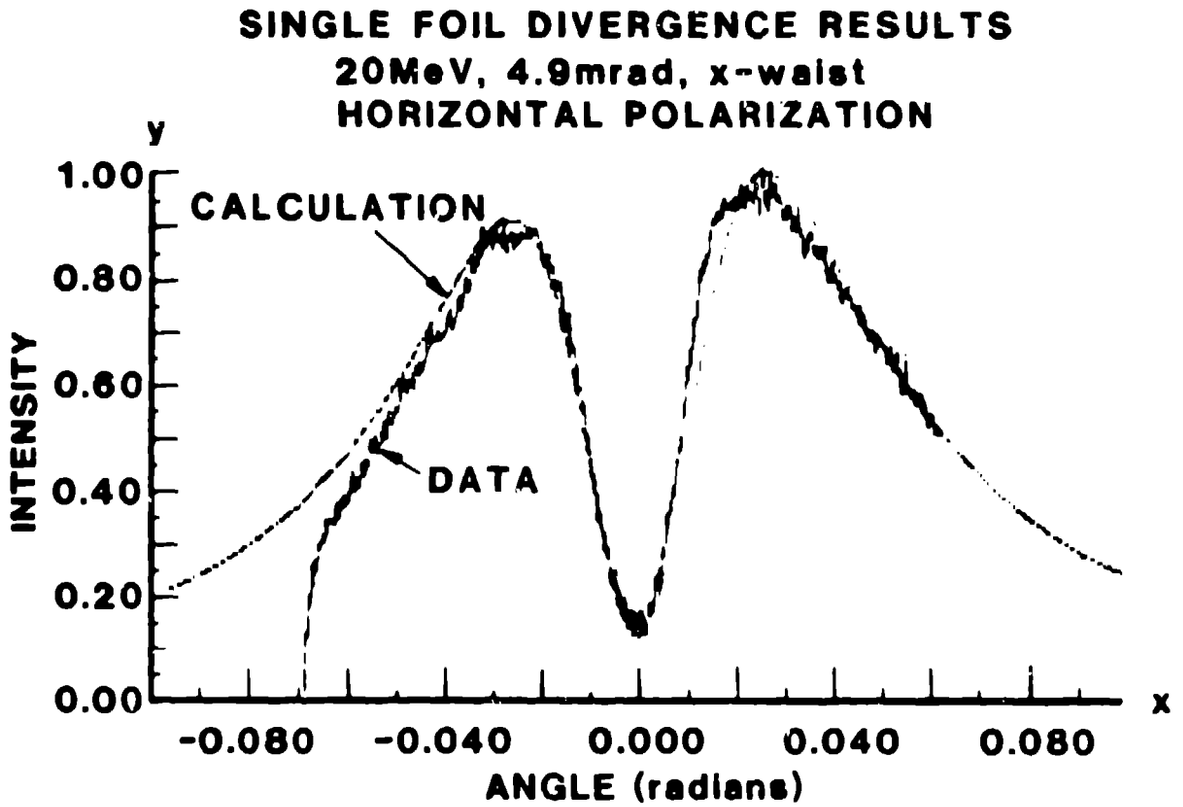
SINGLE FOIL DIVERGENCE RESULTS
20MeV, 4.9mrad, x-waist
HORIZONTAL POLARIZATION
y
1.00
0.80
0.60
0.40
0.20
0.00
INTENSITY
CALCULATION
DATA
x
-0.080
-0.040
0.000
0.040
0.080
ANGLE (radians)

Fig. 6

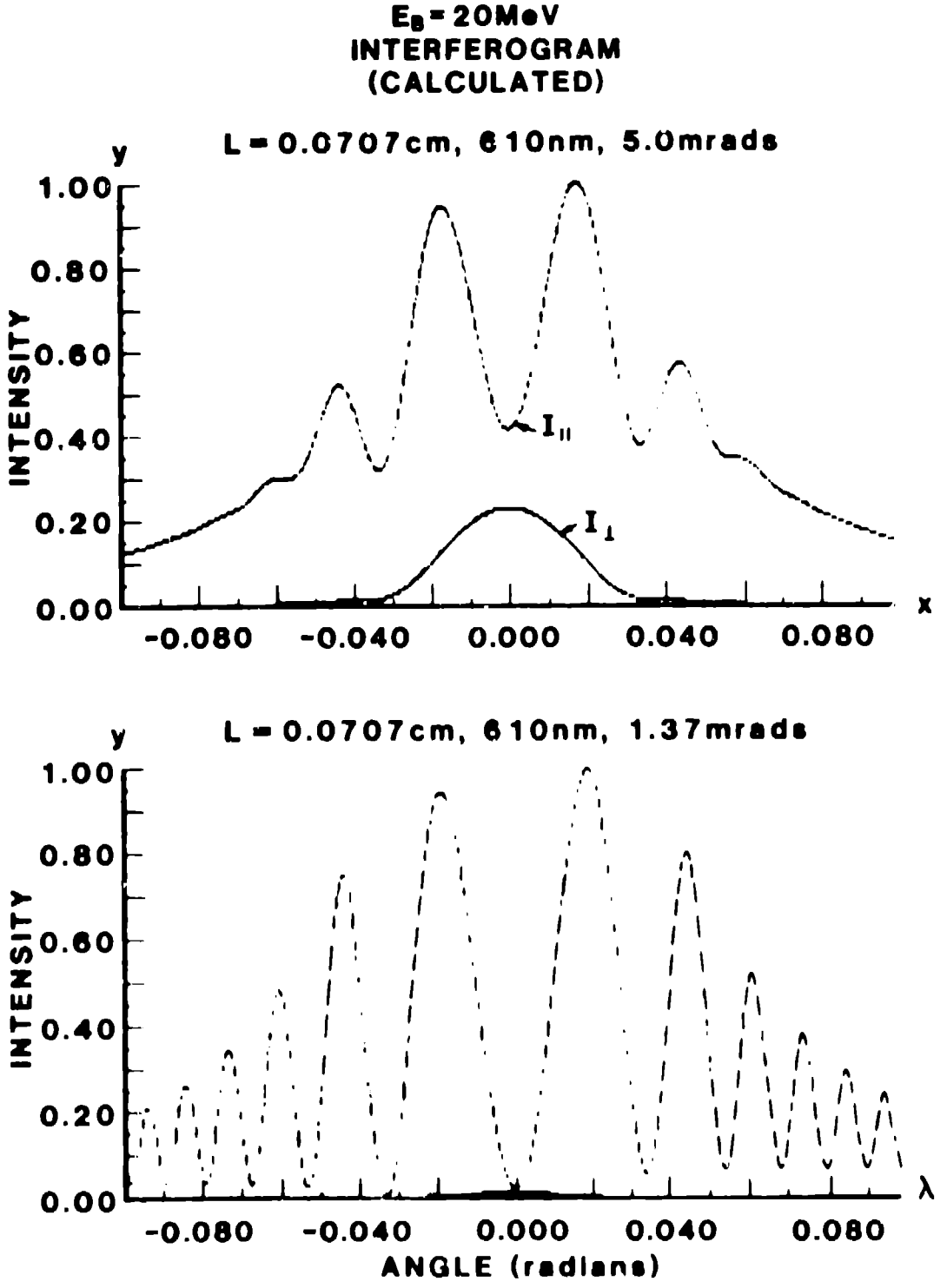
E_B = 20MeV
INTERFEROGRAM
(CALCULATED)
L = 0.0707cm, 610nm, 5.0mrads
y
1.00
0.80
0.60
0.40
0.20
0.00
INTENSITY
I_{II}
$I_{\perp}$
x
-0.080
-0.040
0.000
0.040
0.080
L = 0.0707cm, 610nm, 1.37mrads
y
1.00
0.80
0.60
0.40
0.20
0.00
INTENSITY
λ
-0.080
-0.040
0.000
0.040
0.080
ANGLE (radians)

Fig. 7

Initial Two-Foil Interference Pattern

FOCUS: x,y WAIST
FILTER: 600 x 40nm
POLAR.: HORIZONTAL

FIRST FOIL: KAPTON

SECOND FOIL: ALUMINIZED FUSED SILICA

SEPARATION: 0.5mm NORMAL
0.7mm @ 45°

Fig. 8

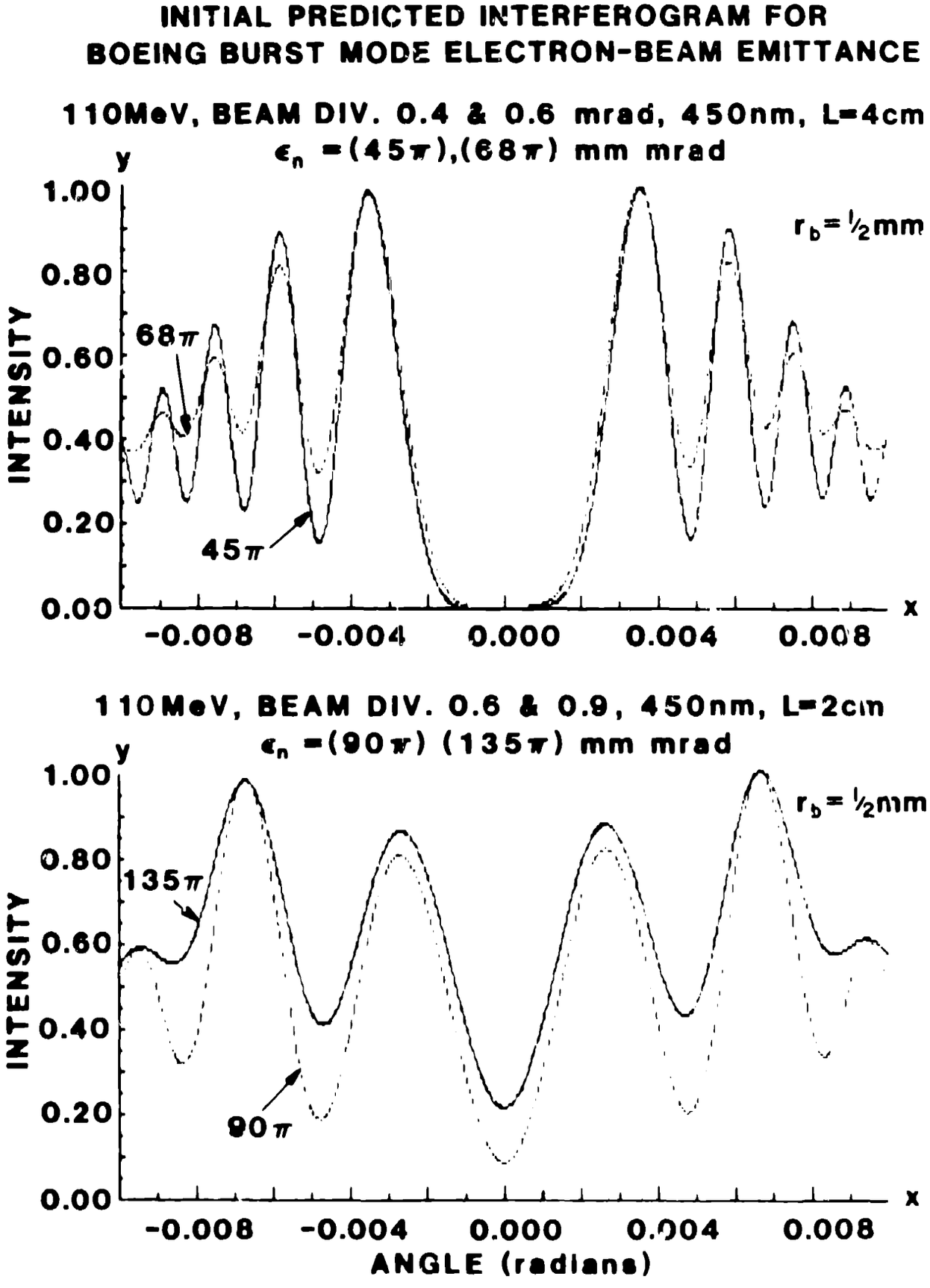
INITIAL PREDICTED INTERFEROGRAM FOR
BOEING BURST MODE ELECTRON-BEAM EMITTANCE
110MeV, BEAM DIV. 0.4 & 0.6 mrad, 450nm, L=4cm
ϵ_n =(45π),(68π) mm mrad
y
1.00
0.80
0.60
0.40
0.20
0.00
INTENSITY
68π
45π
r_b = ½mm
x
-0.008
-0.004
0.000
0.004
0.008
110MeV, BEAM DIV. 0.6 & 0.9, 450nm, L=2cm
ϵ_n =(90π) (135π) mm mrad
y
1.00
0.80
0.60
0.40
0.20
0.00
INTENSITY
135π
90π
r_b = ½mm
x
-0.008
-0.004
0.000
0.004
0.008
ANGLE (radians)

Fig. 9